Catalytic coatings on steel for low-temperature propane prereforming to solid oxide fuel cell (SOFC) application

Pierre Alphonse, Florence Ansart

Catalytic coatings on steel for low-temperature propane prereforming to solid oxide fuel cell (SOFC) application

Pierre Alphonse *, Florence Ansart

Université de Toulouse, CIRIMAT UPS-CNRS, 118 route de Narbonne, 31062 Toulouse Cedex 9, France

Keywords:
Coating
Colloid
PEG
Steam reforming
Fuel processing

A B S T R A C T

Catalyst layers (4–20 μm) of rhodium (1 wt%) supported on alumina, titania, and ceria–zirconia ($Ce_{0.5}Zr_{0.5}O_2$) were coated on stainless-steel corrugated sheets by dip-coating in very stable colloidal dispersions of nanoparticles in water. Catalytic performances were studied for low-temperature (⩽500 °C) steam reforming of propane at a steam to carbon ratio equal to 3 and low contact time (≈0.01 s). The best catalytic activity for propane steam reforming was observed for titania and ceria–zirconia supports for which propane conversion started at 250 °C and was more than three times better at 350 °C than conversion measured on alumina catalyst. For all catalysts a first-order kinetics was found with respect to propane at 500 °C. Addition of PEG 2000 in titania and ceria–zirconia sols eliminated the film cracking observed without additive with these supports. Besides, the PEG addition strongly expanded the porosity of the layers, so that full catalytic efficiency was maintained when the thickness of the ceria–zirconia and titania films was increased.

1. Introduction

Solid oxide fuel cells (SOFC), due to their high working temperature, have some internal reforming ability. However, it has been shown that direct use of hydrocarbons higher than CH_4 to feed a nickel-based anode caused carbon deposition (coke) followed by a catalyst deactivation [1]. Thus, feeding a SOFC with common fuels (natural gas, gasoline, etc.) will require a prereforming unit in order to convert hydrocarbons in a mixture of smaller molecules such as H_2, CH_4, CO, and CO_2, compatible with the nickel anode catalyst of a medium-temperature SOFC [2]. The conversion of hydrocarbon fuels into hydrogen-rich mixtures can be carried out by several reaction processes, including steam reforming, partial oxidation, and autothermal reforming [3]. But only the steam-reforming process can reach hydrogen concentrations above 75% in the dry product gas [4], leading to the best FC efficiency [5]. However, because the steam-reforming reaction is strongly endothermic, heat transfer restrictions will lead to a temperature drop at the reaction site. This will lower reaction rate but will also increase the risk for carbon deposition blocking the active sites.

Enhanced heat and mass transfer can be obtained by using metallic structured reactors. These devices are built by stacking metallic plates incorporating narrow parallel channels coated with a thin layer of catalyst [6–8]. Furthermore, this reactor design allows thermal coupling between endothermic and exothermic reactions in integrated heat exchangers/reactors [9]. Thus, the energy content of the anodic off gas, mainly unconverted hydrogen from the fuel cell stack, can be recovered in order to supply heat for the endothermic steam-reforming reaction, boosting the overall system efficiency.

Improving heat and mass transfer increases the effective activity and more active catalysts, for example, based on precious metals, can be employed. The most efficient metals for steam reforming of methane on alumina-stabilized magnesia-supported catalysts were reported to be rhodium and ruthenium [10]. Though some authors [11] have found that platinum was actually the best catalyst whatever the support, many other studies have confirmed the high activity of rhodium. With more active catalysts the reaction temperature can be lowered so that less thermally stable oxide supports, like titania, for example, can be used and the reactors can be made of standard stainless steels (less expensive). In most of the studies reported on steam reforming in structured reactors the full conversion of hydrocarbon is reached only from 700 °C. Such a temperature is incompatible with a long-term stability of standard steels.

In this paper we report our work on rhodium catalytic coatings for low-temperature (⩽500 °C) steam reforming of propane. These catalysts were synthesized by sol–gel routes and coated on corrugated stainless-steel sheets by dip-coating. This kind of substrate, used to build heat exchangers, could be interesting for large-scale production of low-cost structured reactors.

Corresponding author. Fax: +33 561 556 163.
E-mail addresses: alphonse@chimie.ups-tlse.fr (P. Alphonse), ansart@chimie.ups-tlse.fr (F. Ansart).
URLs: http://www.cirimat.cnrs.fr/ (P. Alphonse), http://www.liebherr.com/ae/en/default_ae.asp (F. Ansart).

2. Materials and methods

2.1. Sol synthesis

Boehmite sols, precursors of alumina xerogels, were synthesized according to the process originally reported by Yoldas [12–14]. A large excess ($H_2O/Al \approx 100$) of hot (85 °C) distilled water was quickly poured in aluminum tri-sec-butoxide, $Al(OC_4H_9)_3$ under vigorous stirring. After 15 min the hydroxide precipitate was peptized by adding 0.07 mol of nitric acid per mole of alkoxide and stirring at 85 °C until a clear sol was obtained (≈24 h). At this stage the pH of the sol was 5.0 ± 0.5. After peptization, the sol was concentrated by heating at 85 °C until 2/3 of the solvent has evaporated.

$Ce_{0.5}Zr_{0.5}O_2$ sols were synthesized by a method based on that reported by Deshpande et al. [15]. The first step was the hydrolysis of the mixed precursors ($Ce(NO_3)_6(NH_4)_2$, and $ZrO(NO_3)_2{\cdot}xH_2O$) by addition of an aqueous NH_3 solution up to pH >10. The precipitate was thoroughly washed and then it was peptized (by addition of 0.6 mol of nitric acid per mole of Ce + Zr) until a clear sol was obtained (≈48 h). At this stage the pH of the sol was 2.0 ± 0.5. The peptization time can be shortened by sonication. The sols were then concentrated by ultrafiltration (using MWCO 2000 dialysis membranes).

Titania sols were prepared by hydrolysis of titanium alkoxide in a large excess of water. This method can give colloids of titania nanocrystallites dispersed in water [16,17]. The following procedure was optimized to produce very stable sols. Hot (80 °C) distilled water ($H_2O/Ti \approx 90$) was added quickly, under vigorous stirring, on titanium(IV) isopropoxide dissolved in isopropyl alcohol ($C_3H_8O/Ti = 3.5$). A white precipitate was obtained. After 5 min, a solution of nitric acid ($H^+/Ti = 0.2$) was added to the suspension and the mixture was kept for 16 h at 80 °C under stirring. The white suspension changed gradually to a translucent sol by peptization. At this stage the pH of the sol was 1.0 ± 0.5. More concentrated sols were obtained by evaporation at the same temperature until the required concentration was reached.

For the three kinds of sol, the rhodium precursor ($RhCl_3{\cdot}xH_2O$), dissolved in a minimum amount of water, was added, in suitable proportion, into the sol at the end of the peptization step. Then the sol was stirred at room temperature for 1 h. These sols remained stables (no precipitation) for more than 1 year.

2.2. Powder X-ray diffraction (PXRD)

The crystal structure was investigated by powder X-ray diffraction. Data were collected, at room temperature, on a Seifert 3003TT θ–θ diffractometer in Bragg–Brentano geometry, using filtered Cu Kα radiation and a graphite secondary-beam monochromator. Diffraction intensities were measured by scanning from 20° to 80° (2θ) with a step size of 0.02° (2θ). Crystalline structures were refined using FullProf software [18]. The peak profiles were modeled by pseudo-Voigt functions. The refined FWHM (full-width at half-maximum) of the lines was used to compute, by the Scherrer's equation, the average crystallite size [19]. The instrumental broadening contribution was measured by using a highly crystalline rutile sample as standard.

2.3. Specific surface area, PSD, and density

The specific surface areas were computed from the adsorption isotherms, using the Brunauer–Emmett–Teller (BET) method [20]. Adsorbate was nitrogen for xerogels. Krypton was used for coatings which were done on both sides of a set of four small stainless-steel sheets (20 × 15 mm) because the sheets used in the steam-reforming reactor were too large to fit in adsorption cells. Isotherms were recorded at 77 K, with a Micromeritics ASAP 2010M. The pore size distributions (PSD) were computed from nitrogen desorption isotherms by the NLDFT method [21] (with Quantachrome Autosorb-1 software using silica equilibrium transition kernel at 77 K, based on a cylindrical pore model).

Skeletal densities of powder were determined using a gas pycnometer (Micromeritics AccuPyc 1330) and working with helium. Each experimental value results from the average of 10 successive measurements on the same sample.

2.4. Thermal analyses

Simultaneous thermogravimetric (TG) and differential thermal (DT) analyses were carried out on a SETARAM TG-DTA 92 thermobalance using 20 mg of sample; α-alumina was taken as reference.

2.5. Electron microscopy

Transmission electron microscopy (TEM) analyses were done on a JEOL 2010. Samples were prepared by dipping a carbon-coated grid in a sol diluted 50 times in water. Then the grid was allowed to dry 48 h at room temperature. Scanning electron microscopy (SEM) analyses were done, with a JEOL JSM-6700F, on small pieces cut in coated substrates.

2.6. Coating of stainless-steel substrates

The corrugated-steel sheets used in this work were made by the Liebherr-Aerospace Company[1] for their heat exchangers. The steel grade was AISI 321 with a square-wave profile; the sheet thickness was 0.1 mm and the channel width was 1 mm.

In order to ensure an optimal adhesion between the layer and the substrate, the stainless-steel plates were immersed in an alkaline cleaner (TurcoTM 4181) at 75 °C for 30 min before the coating. Then they were rinsed with water in an ultrasonic bath. Finally they were dried and heated in air at 500 °C for 2 h. The catalyst layers were applied by dip-coating using a NIMA DC-mono dip-coater. The thickness of the coating was mainly controlled by the sol concentration, the withdrawal rate being kept constant at 10 mm/min. The amount of catalyst coated on the plates has been evaluated by weighting before and after the coating. From this value, the density and the porosity of the layer, an average thickness has been estimated by the equation

$$t = \frac{W}{\rho[1-\varphi]}\frac{1}{S}, \tag{1}$$

where t is the thickness in cm, W is the catalyst mass in g, ρ is the crystal density in g/cm^3, φ the porosity, and S is the coating area in cm^2.

2.7. Test rig for propane steam-reforming reaction

Propane and argon were dosed by mass flow controllers (Brooks 5850). The water was dosed by an HPLC pump (Knauer Wellchrom K1001) and injected in the propane-argon mixture preheated at 150 °C. Fig. 1 shows a picture of the open testing reactor containing one structured sheet (10 cm length, 5 cm wide, and 1 mm deep). The reactor was designed for containing more than one sheet but the results reported in this paper were obtained by using only one sheet. The free space was filled by nonstructured steel plates with the same dimensions. Thus, the structured sheet was tightly enclosed and the inlet stream was constrained to flow through

[1] http://www.liebherr.com/ae/en/default_ae.asp.

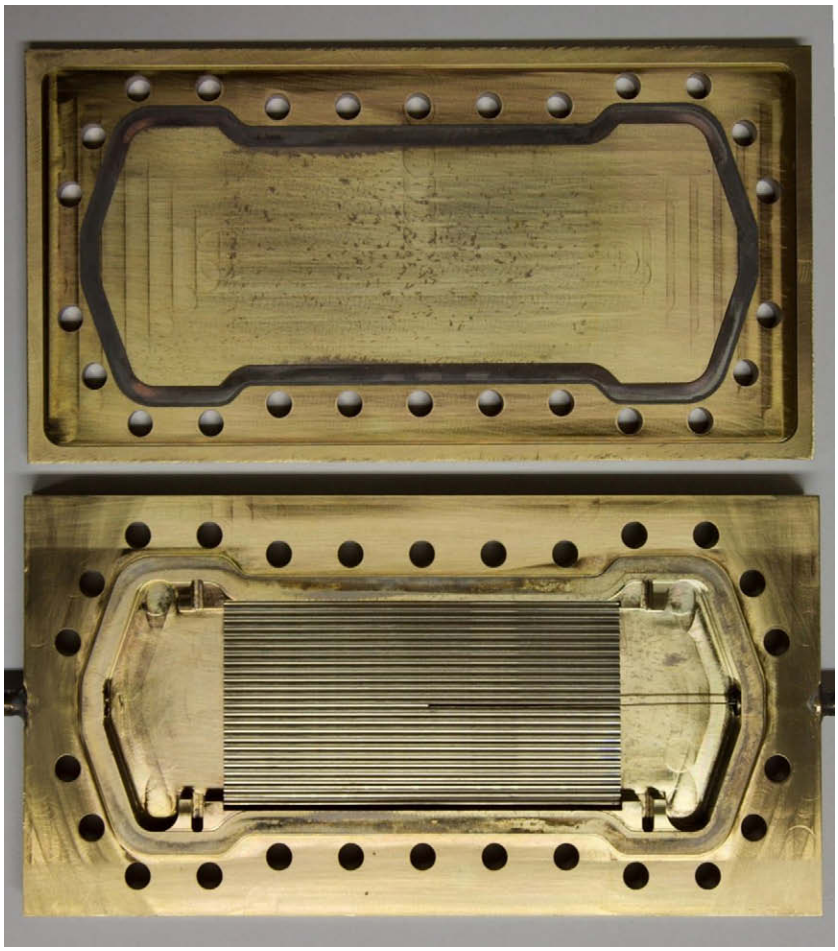

Fig. 1. Testing reactor; the structured sheet dimensions are length = 100 mm, width = 50 mm, and depth = 1 mm.

the channels coated with catalyst. All materials, included the inlet and outlet tubes, were made of stainless steel (ASI 316L). The reactor was closed by a set of screws and nuts. Tightness was obtained thanks to a copper gasket. The reactor was heated by two resistive elements (2×500 W). The temperature of the reactor was measured by a K-type thermocouple placed against the external wall. The temperature of the structured sheet was measured by another K-type thermocouple located in the central channel (see Fig. 1).

The outlet gas stream was first sampled by a quadrupole mass spectrometer (Hiden HPR-20 QIC gas analysis system) and then it was analyzed by IR spectrometry (Nicolet 510P FTIR spectrometer) using a home-made gas cell (KBr windows, optical path length of 10 cm, internal volume of 10 cm^3). All experiments were done at atmospheric pressure using a steam to carbon ratio (S/C) of 3 and a total inlet flow rate of 6.7 L/h (dry basis).

The reaction rate, r, is given by the expression [22]

$$r = F_{C_3H_8} \frac{d(X_{CH_3H_8})}{d(W_{Rh})}, \tag{2}$$

where $F_{C_3H_8}$ is the inlet flow of propane, $X_{C_3H_8}$ the conversion of propane, and W_{Rh} the rhodium mass in the catalyst.

3. Results and discussion

3.1. Characterization of xerogels dried at room temperature

In order to obtain enough material for the microstructural characterizations, a layer of sol was deposited on a PTFE substrate. After drying at room temperature, a thin film of xerogel, which could be easily separated from the substrate, was obtained.

The sols prepared by the Yoldas process are essentially composed of nanosized crystals of boehmite, AlOOH. The crystallites are in the shape of platelets or disks with a thickness of about 3 nm and a diameter in the range 6–9 nm [23].

The XRD pattern of ceria–zirconia xerogels shows very broad diffraction peaks (Fig. 2a). Refinement of the structure by the Rietveld method, using a cubic fluorite-type phase (space group Fm-3m) leads to a good agreement between observed and calculated profiles. The crystallite size calculated from the peak width, using the Scherrer equation, is about 2 nm. The particle size evaluated from the TEM image (Fig. 3 top) is in the range 2–3 nm. These values are in good agreement with those reported by A. Deshpande et al. [15].

As shown by XRD patterns (Fig. 4a) titania xerogels contain two crystalline phases, anatase (tetragonal, $I4_1/amd$) and brookite (orthorhombic, Pbca). Because of the numerous brookite reflections, and the strong overlap of the diffraction lines (because phases are nanocrystalline), we failed to find an acceptable solution by the Rietveld method. However, analysis of the patterns with the profile matching method (whole-pattern decomposition) gave the cell parameters and the peak profiles for both phases. From the peak width we found 6 nm as average size of anatase crystallites and 5 nm for the size of brookite crystals. These values are in agreement with the size which can be estimated from the TEM image (Fig. 3 bottom). As already reported by Zhang and Banfield [24], to determine the phase proportions of anatase and

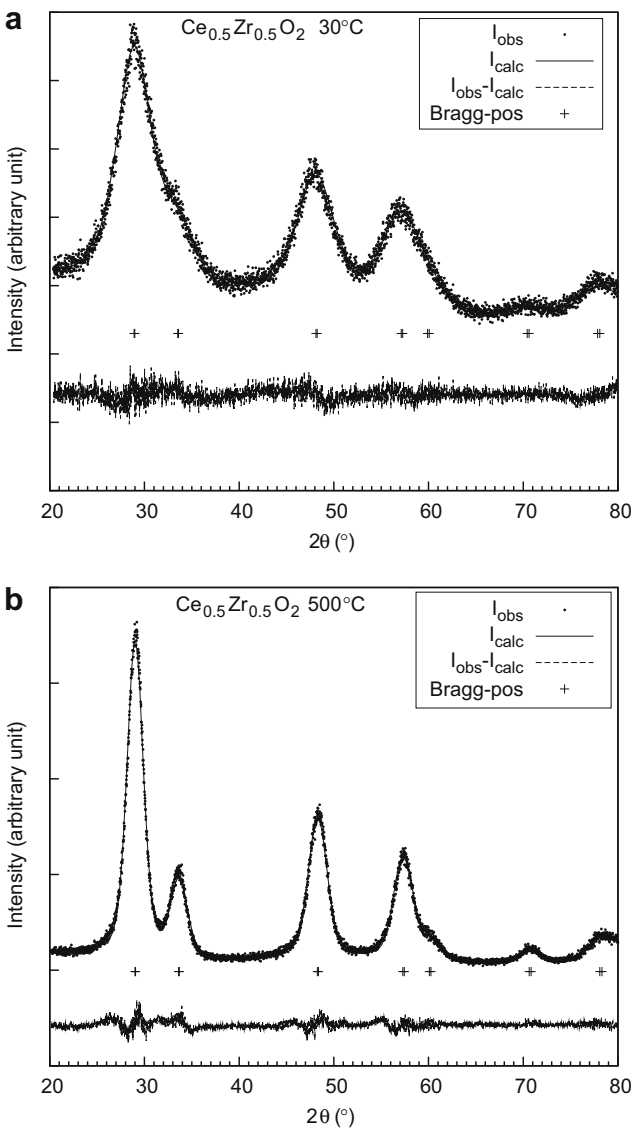

Fig. 2. Experimental XRD pattern (dots) and Rietveld refinement (cubic fluorite-type unit cell, space group No. 225, Fm-3m) for ceria–zirconia xerogel: (a) dried at 30 °C; (b) fired at 500 °C.

brookite, refinement of the structure by the Rietveld method was done with a 2θ range restricted to 20–35°(2θ). This range includes the (1 0 1) line of anatase, and (1 2 0), (1 1 1), (1 2 1) lines of brookite. For the refinement, all parameters except the scale factors were fixed. We found by this method that brookite fraction in the mixture was close to 30%.

3.2. Characterization of xerogels fired at 500 °C

To study the microstructure at the maximum working temperature of the catalysts, the xerogels were fired in air at 500 °C for 2 h. For boehmite this thermal treatment induces the transformation in γ-alumina (Fig. 5). For ceria–zirconia xerogels no structural change occurs (Fig. 2b), but a significant increase of the crystallite size from 2 to 4 nm. It is interesting to note that this mixed oxide seems quite stable given that phase segregation was never observed even after calcination at 800 °C.

In the case of titania xerogels, heating at 500 °C begins to induce the transformation of both anatase and brookite in the more thermodynamically stable rutile phase (tetragonal, space group $P4_2/mnm$). Fig. 4b shows that this transformation is accompanied by a strong increase of the crystallinity. The proportion and the crystal size for each phase are reported in Table 1.

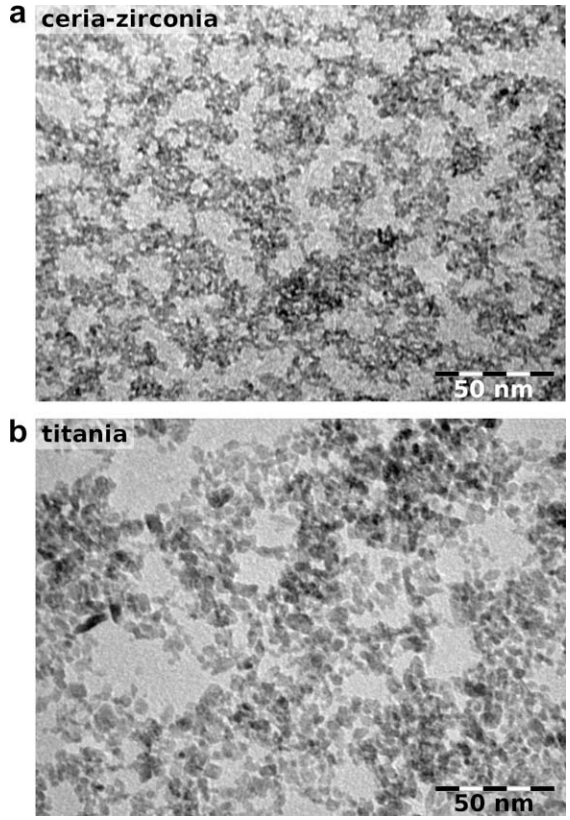

Fig. 3. TEM images of xerogels dried at 30 °C: (a) ceria–zirconia xerogel; (b) titania.

Nitrogen adsorption isotherms reveal that all catalysts are essentially mesoporous (Fig. 6a). The porous volumes of ceria–zirconia and titania catalysts are three times lower than the porous volumes of alumina catalysts (Table 2). The pore size distributions (PSD) were computed from desorption isotherms by the NLDFT method (Fig. 6b). For ceria–zirconia the PSD shows only one narrow peak with a maximum at 3.3 nm. For titania catalysts, the distribution is broader with a maximum at 6.4 nm and a small shoulder at 4.6 nm. For alumina catalysts the PSD shows roughly two main peaks at 4.4 and 5.6 nm.

The BET specific surface area is 330 m^2/g for alumina, 140 m^2/g for ceria–zirconia, and 60 m^2/g for titania catalysts.

The surface areas of stainless-steel sheets, coated on both sides with the three kinds of sols, were measured, after calcination at 500 °C, by krypton adsorption at 77 K. The surface areas divided by the mass of the film were in good agreement with the specific surface areas measured with unsupported xerogels dried on PTFE substrates.

It was reported that addition of polyethylene glycol (PEG) in titania hydrosols can significantly improve the surface area and the porosity of the xerogels [25,26]. Thus, in order to increase the low porosity of ceria–zirconia and titania xerogels, various amounts of PEG 2000 were added into the sols after peptization. It should be noted that when PEG was added before peptization, it had a lesser effect on surface area and pore volume; moreover, for a EO/Ti ratio larger than 1.0, the sols were no more stable. The modifications of pore volume and BET specific surface area induced by addition of PEG 2000 are reported in Table 3. Indeed the PEG addition increased almost three times the pore volume for ceria–zirconia and four times for titania. The BET surface area was increased more than two times for titania whereas the gain was only

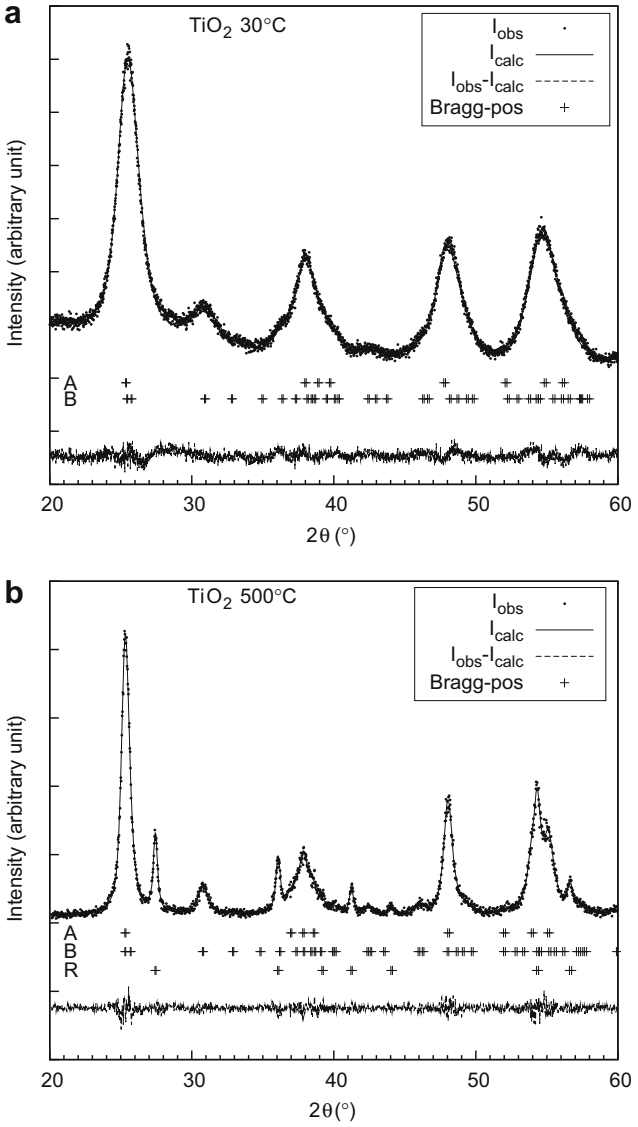

Fig. 4. Experimental XRD pattern (dots) and whole pattern decomposition for titania xerogels. (a) Xerogel dried at 30 °C. Refinement was done for a mixture of anatase (A: tetragonal unit cell, space group No. 141, $I4_1/amd$) and brookite (B: orthorhombic unit cell, space group No. 61, Pbca). (b) xerogel fired at 500 °C in air. Refinement was done for a mixture of anatase (A: tetragonal unit cell, space group No. 141, $I4_1/amd$), brookite (B: orthorhombic unit cell, space group No. 61, Pbca), and rutile (R: tetragonal unit cell, space group No. 136, $P4_2/mnm$).

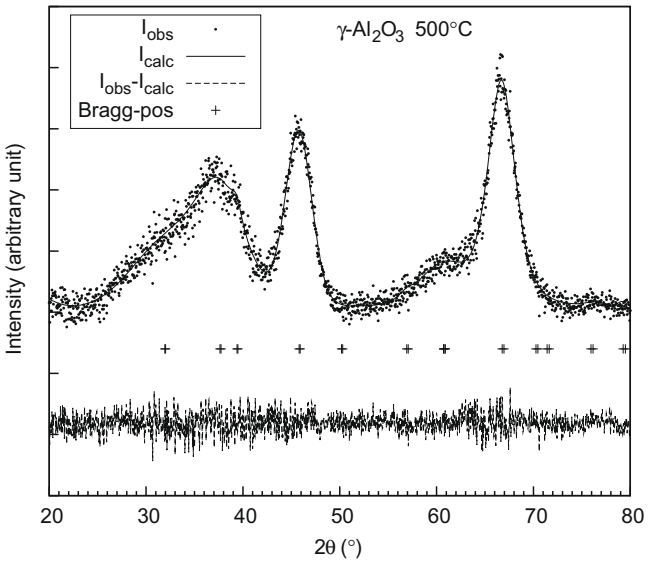

Fig. 5. Experimental XRD pattern (dots) for an alumina xerogel fired at 500 °C in air for 2 h and Rietveld refinement (cubic spinel-type unit cell, space group No. 227, Fd-3m).

Table 1
Effect of temperature on phase concentrations and crystal size for titania-supported catalysts.

	Xerogel dried at 30 °C		Xerogel fired at 500 °C	
Crystalline phase	%	Size (nm)	%	Size (nm)
Anatase	70	6	65	15
Brookite	30	5	25	11
Rutile	0	–	10	31

20% for ceria–zirconia. There is an optimum value for the amount of PEG, above which the porosity and the surface area decrease, and this optimum seems similar for both supports. Addition of PEG induces an increase of the number of pores, a shift toward larger pore size, and a broadening of the pore size distributions (Fig. 7).

In the case of titania and ceria–zirconia, the film adhesion was not good compared to alumina. As the layers were transparent, for alumina it was often difficult to see with the naked eye the difference between a coated plate and an uncovered one, whereas the ceria–zirconia and titania coatings were always severely cracked. Frequently the layer peeled off from the substrate and the coating operation should be done again. We found that addition of PEG 2000 into the sols not only increased the porosity but also improved significantly the coating adhesion. Probably with the less compact layers synthesized with PEG, the stress due to the thermal expansion difference between the ceramic film and the metallic substrate is reduced when the plates are heated.

The SEM images of the coatings on the metallic plates are shown in Fig. 8. Whatever the material, the catalyst layers appear very homogeneous with no macroporosity, especially in the case of the ceria–zirconia layer. The alumina catalyst, thanks to its fibrous structure, has a less compact arrangement which explains its larger pore volume.

EDX analysis indicated that rhodium was uniformly distributed in the catalysts. It was impossible to detect the presence of rhodium particles neither in the X-ray diffraction patterns nor on the TEM images. A more detailed analysis of these xerogels is in progress.

For a catalyst mass of 0.03 g, the average thickness of the layer, calculated by Eq. (1), is about 9 μm for alumina ($\rho = 3.2$, $\varphi = 0.48$), 4 μm for ceria–zirconia ($\rho = 6.5$, $\varphi = 0.38$), and 5 μm for titania ($\rho = 3.7$, $\varphi = 0.24$).

3.3. Catalyst activity for propane steam reforming

The influence of temperature on catalytic activity and product distribution of propane steam reforming, over one microstructured sheet coated with 1% Rh/alumina catalyst, is shown in Fig. 9, where propane and product concentrations are plotted against reaction temperature. It can be seen that conversion of propane starts from 360 °C and complete conversion is achieved at 430 °C. The reaction products are hydrogen, carbon monoxide, carbon dioxide, and

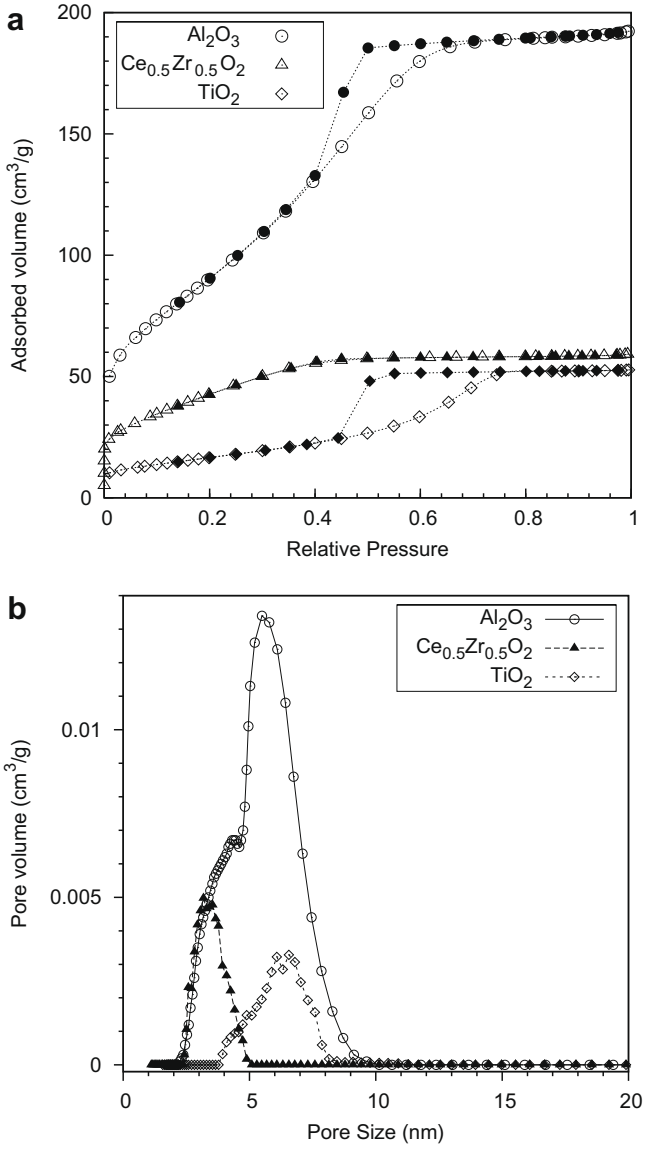

Fig. 6. (a) Nitrogen adsorption–desorption isotherms of catalyst xerogels (fired at 500 °C in air for 2 h) recorded at 77 K (open symbols denote adsorption and solid symbols desorption). (b) Pore size distributions computed from nitrogen desorption isotherms by the NLDFT method with Quantachrome Autosorb-1 software using silica equilibrium transition kernel at 77 K, based on a cylindrical pore model.

Table 2
Porosity and BET surface area of catalysts xerogels fired at 500 °C in air for 2 h.

	Alumina	Ceria–zirconia	Titania
Pore volume (cm^3/g)	0.30	0.09	0.08
Porosity (%)	48	38	24
BET surface area (m^2/g)	330	140	60

methane. No other by-products were detected. Propane steam reforming consists of three reactions:

$$C_3H_8 + 3H_2O \rightarrow 3CO + 7H_2, \quad (3)$$

$$C_3H_8 + 6H_2O \rightarrow 3CO_2 + 10H_2, \quad (4)$$

$$CO + H_2O \leftrightarrow CO_2 + H_2. \quad (5)$$

The two reforming reactions (3) and (4) are strongly endothermic and can be considered as irreversible, whereas the third called water–gas shift reaction (WGS) is reversible and exothermic. Methane can be produced either by hydrogenation of carbon monoxide or carbon dioxide (methanation) as shown in reactions (6) and (7) or by hydrogenation of adsorbed C_1 carbon species [27].

Table 3
Effect of PEG 2000 addition on pore volume and BET surface area for ceria–zirconia and titania-supported catalysts after calcination at 500 °C for 2 h.

	Pore volume (cm^3/g)	Porosity (%)	BET surface area (m^2/g)
$Ce_{0.5}Zr_{0.5}O_2$ – EO/ZC = 0	0.09	38	160
$Ce_{0.5}Zr_{0.5}O_2$ – EO/ZC = 2.0	0.23	61	200
$Ce_{0.5}Zr_{0.5}O_2$ – EO/ZC = 3.0	0.20	58	190
TiO_2 – EO/Ti = 0	0.08	24	60
TiO_2 – EO/Ti = 1.2	0.27	52	130
TiO_2 – EO/Ti = 1.8	0.31	55	140
TiO_2 – EO/Ti = 2.4	0.26	51	125

The amount of PEG is expressed as the number of ethylene oxide (EO) units per metal oxide.

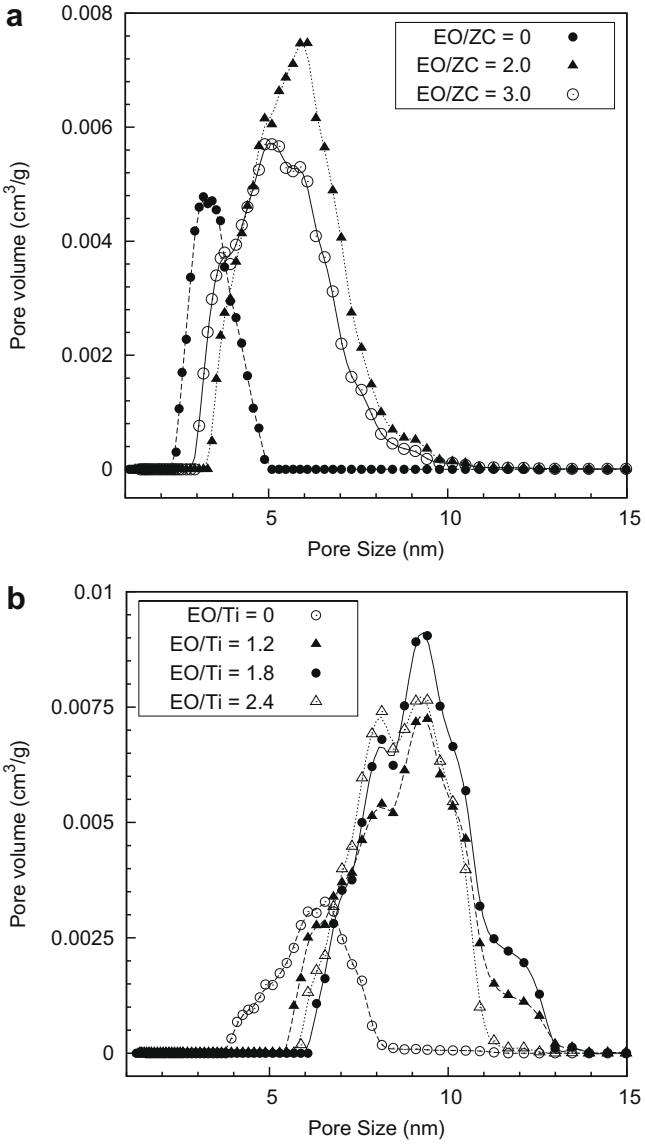

Fig. 7. Effect of PEG 2000 addition on pore size distributions (PSD) of xerogels fired at 500 °C in air for 2 h. PEG amount is expressed as the number of ethylene oxide (EO) units per metal oxide. PSD were computed by the NLDFT method. (a) Ceria–zirconia-supported catalysts; (b) titania-supported catalysts.

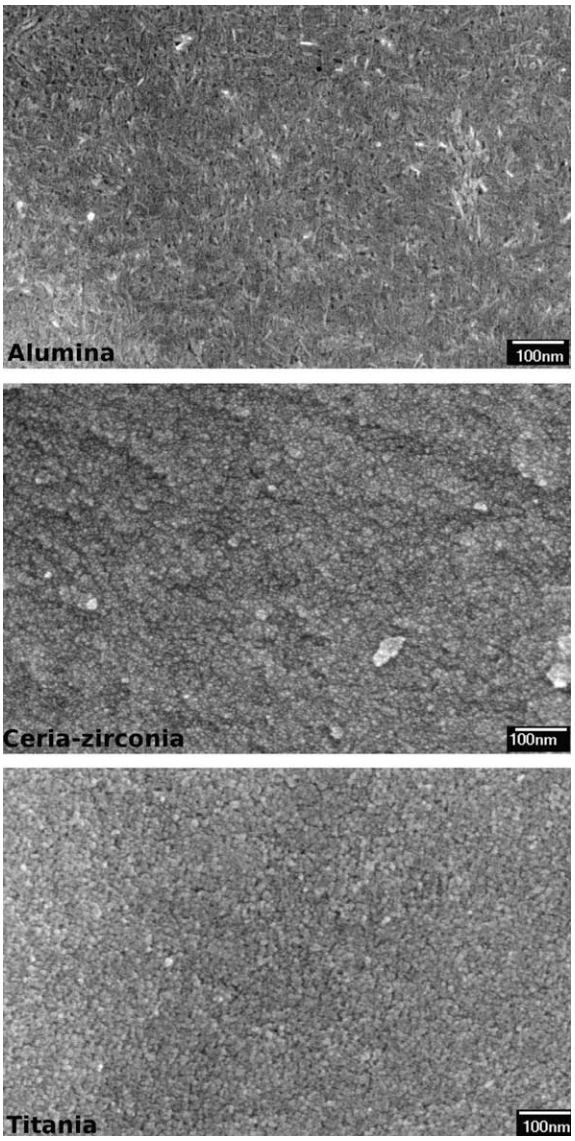

Fig. 8. SEM images of the coatings fired at 500 °C in air for 2 h.

$$CO + 3H_2 \leftrightarrow CH_4 + H_2O, \quad (6)$$

$$CO_2 + 4H_2 \leftrightarrow CH_4 + 2H_2O. \quad (7)$$

It was observed that addition of hydrogen in the inlet flow had almost no effect on propane conversion and CO concentration, but increased methane formation (see Table 4). It was recently established that, in steam reforming of ethane on Rh/YSZ catalysts [28], methanation did not significantly contribute to the formation of methane which was mainly produced by ethane hydrogenolysis.

The data reported in Fig. 9 were recorded on a fresh catalyst. No activation under hydrogen was done before the test. When the catalyst has already worked, the conversion of propane starts at a lower temperature (about 320 °C) (see Fig. 10). A decrease of reaction rate occurs from 380 °C and, from this temperature, the formation of methane is observed. The CO and CO_2 concentrations remain similar which indicates that the WGS equilibrium is not reached under these conditions (for example, at 400 °C, the CO/CO_2 equilibrium ratio is about 0.2).

In Fig. 10, propane conversion ($X_{C_3H_8}$) versus temperature is compared for three structured sheets coated with the three kinds of rhodium catalysts. The catalyst mass, and thus the amount of rhodium, was similar for the three coatings. It is clear that, for pro-

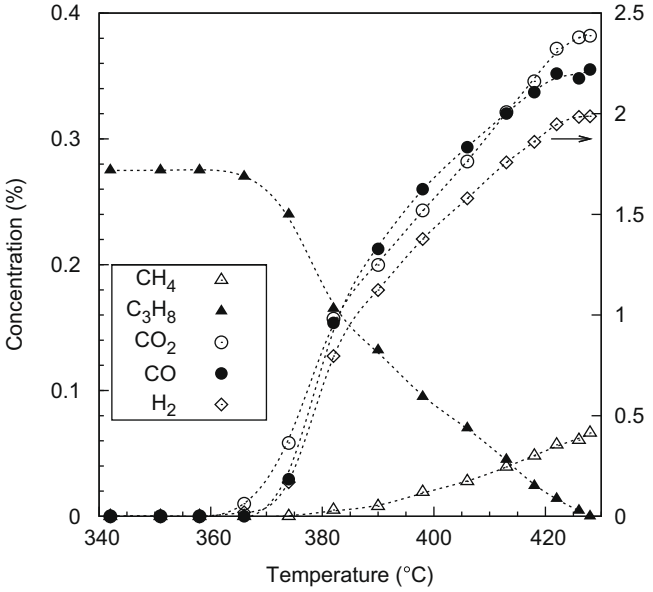

Fig. 9. Effect of temperature on propane conversion and product distribution for an alumina-supported catalyst. S/C = 3, total inlet flow rate = 6.7 L/h (dry basis), and catalyst mass = 0.03 g.

Table 4
Effect of hydrogen addition in the inlet flow on propane conversion and product distribution.

H_2 concentration in inlet (%)	C_3H_8 conversion (%)	CH_4 concentration in outlet (%)	CO_2 concentration in outlet (%)	CO concentration in outlet (%)
0.0	76	0.03	0.25	0.27
0.7	75	0.05	0.22	0.27
3.0	76	0.26	0.12	0.25

Temperature = 400 °C, S/C = 3, total inlet flow rate = 6.7 L/h (dry basis), 1% Rh/Alumina catalyst, catalyst mass ≈ 0.03 g.

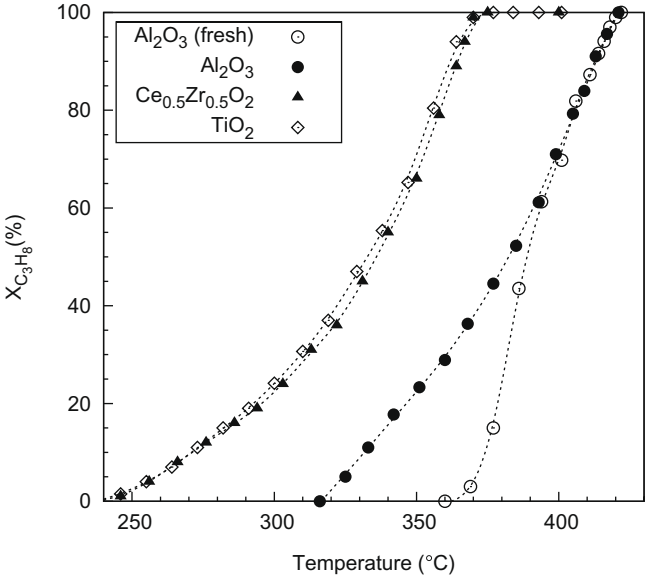

Fig. 10. Effect of the catalyst support on propane conversion. S/C = 3, total inlet flow rate = 6.7 L/h (dry basis), and catalyst mass ≈ 0.05 g.

pane steam reforming, the oxide carrier has a strong effect on the catalytic activity. On ceria–zirconia and titania-supported catalysts, propane conversion started from 250 °C and complete conversion was achieved as soon as 370 °C. At 350 °C the conversion measured for the ceria–zirconia and titania catalysts was more three times better than that for alumina catalyst (Table 5).

The reaction rate followed an Arrhenius law and apparent activation energy can be evaluated. We found about 80 kJ/mol for alumina, 66 kJ/mol for ceria–zirconia, and 63 kJ/mol for titania (Table 5). These values are consistent with those (≈80 kJ/mol) reported for steam reforming of hydrocarbons higher than methane, on nickel-based catalysts [22].

As noted before, and shown in Fig. 10 for alumina, propane conversion started always at higher temperatures for a fresh catalyst. This inhibition period, observed for all kinds of supports (however in less extent than for alumina), disappeared after an activation at 350 °C under hydrogen before the first catalytic test. Thus, with these rhodium catalysts, the reduction in hydrogen is not mandatory to reach the full activity. It is interesting because if the catalysts are contacted with air (for example, for regeneration) a hydrogen supply is not required to recover the activity.

The ratio between the CO and the CO_2 concentrations, as well as the amount of CH_4 formed, strongly depends on the catalyst carrier (Table 6). The CO/CO_2 ratio is close to the WGS equilibrium only for the titania catalyst. For ceria–zirconia the ratio is lower whereas it is higher for alumina.

Previous work on steam reforming of hydrocarbons showed that the catalyst support had an effect not only on the rate of catalytic activity but also on the type and quantity of products formed [29]. However, Wei and Iglesia demonstrated recently that, in the temperature range 550–750 °C, the rate-determining step of CH_4 steam reforming is the C–H bond activation [30,31]. As this reaction is known to occur only on metal sites, this implies that the support has no effect on the reaction rate. They stated that the numerous results reported in the literature claiming the effect of catalyst support are sometimes contradictory and can be explained by transport artifacts or difference in metal dispersion. Nevertheless, besides its influence on metal dispersion, it is known that the support can also modify the carbon deposition. For example, acidic supports will promote cracking and polymerization leading to carbon formation. A support such as MgO can reduce the coke formation because of both its basicity and its ability to enhance steam adsorption. On the other hand supports like ZrO_2 or CeO_2 are also able of oxidizing deposited carbon by using lattice oxygen.

In our experiments mass and heat transfer limitations can be excluded because we used diluted feeds and thin layers of catalyst on metallic substrates. The lower activity observed with alumina support can be explained by several causes. Though it was not yet measured, it is highly probable that the rhodium dispersion and accessibility will be different on alumina because rhodium precursors should cope with the structural transformation of boehmite in γ-alumina. Moreover, alumina is highly acidic and there is no possibility of oxygen transfer from the support; thus the number and nature of surface carbon species will be strongly different. This is reflected by the significant differences observed in experimental CO/CO_2 ratio.

In the upper part of Table 7, the reaction rate (mmol of propane converted per second and per gram of Rh) measured at 350 °C is compared for several microstructured sheets coated with 1% Rh/$Ce_{0.5}Zr_{0.5}O_2$ catalyst. For the same mass of catalyst, addition of PEG had little impact on reaction rate. But, if the catalyst amount is increased (i.e., the thickness is increased), without the addition of PEG the reaction rate strongly decreases, whereas it does not change significantly if PEG were added. As ceria–zirconia has a low porosity without PEG, when the catalyst layer is thicker only the upper part of the coating is working efficiently. This limitation is overcome by the large increase of porosity induced by the PEG addition. On the other hand, as the surface area enhancement brought by PEG is low, this could explain why addition of PEG does not improve significantly the reaction rate. The same behavior is observed for titania catalysts (Table 7). However, in this case, a lar-

Table 5
Comparison of activation energies and propane conversion observed at 350 °C.

	Alumina	Ceria–zirconia	Titania
Activation energy (kJ/mol)	81	66	63
Temperature range (°C)	342–409	276–350	273–347
Propane conversion at 350 °C	22	66	70

S/C = 3, total inlet flow rate = 6.7 L/h (dry basis), catalyst mass ≈ 0.06 g.

Table 6
Comparison of CO/CO_2 ratio and % CH_4 observed at 100% conversion of propane.

	Alumina	Ceria–zirconia	Titania
T (°C)	420	370	370
% CH_4	0.07	0.05	0.11–0.13
CO/CO_2	0.7–0.8	0–0.01	0.08–0.12
CO/CO_2 for WGS equilibrium	0.24	0.14	0.12

S/C = 3, total inlet flow rate = 6.7 L/h (dry basis), catalyst mass ≈ 0.05 g.

Table 7
Effect of addition of PEG 2000 on catalytic activity for ceria–zirconia and titania catalysts.

	Catalyst mass (g)	Calculated thickness (μm)	Propane conversion at 350 °C (%)	Reaction rate (mmol s^{-1} g_{Rh}^{-1})
$Ce_{0.5}Zr_{0.5}O_2$ – EO/ZC = 0	0.053	7	66	0.26
$Ce_{0.5}Zr_{0.5}O_2$ – EO/ZC = 0	0.090	11	76	0.18
$Ce_{0.5}Zr_{0.5}O_2$ – EO/ZC = 2.0	0.034	7	44	0.27
$Ce_{0.5}Zr_{0.5}O_2$ – EO/ZC = 2.0	0.059	12	71	0.25
TiO_2 – EO/Ti = 0	0.053	9	70	0.28
TiO_2 – EO/Ti = 0	0.091	16	77	0.18
TiO_2 – EO/Ti = 1.8	0.046	14	61	0.28
TiO_2 – EO/Ti = 1.8	0.064	19	78	0.26

S/C = 3, total inlet flow rate = 6.7 L/h (dry basis). Thickness was calculated with Eq. (1) and reaction rate with Eq. (2). The amount of PEG is expressed as the number of ethylene oxide (EO) units per metal oxide.

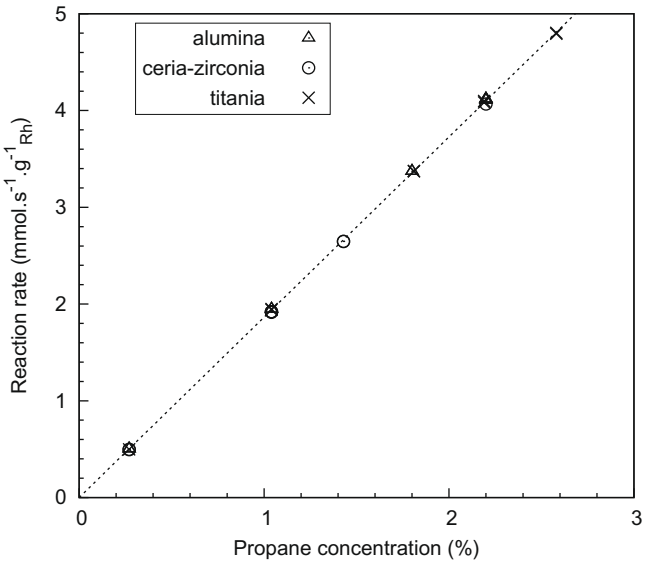

Fig. 11. Effect of propane concentration on reaction rate at 500 °C, S/C = 3, total inlet flow rate = 6.7 L/h (dry basis), and catalyst mass ≈ 0.04 g.

ger reaction rate would have been expected since addition of PEG increases the specific surface area by 230% (Table 3).

Whatever the catalyst carrier, the reaction rate measured at 500 °C, for a S/C ratio fixed to 3, was proportional to propane concentration (Fig. 11). Due to experimental setup limitations (instability in the water vaporization for a steam concentration exceeding 20%), propane concentration in inlet could not exceed 2.6%. For this value hydrogen concentration in outlet flow was 16%. This gives a minimum of 260 g of hydrogen produced per gram of rhodium and per hour. To our knowledge no hydrogen production value has been reported for propane steam reforming at 500 °C. A value of 1575 g of hydrogen produced per gram of rhodium and per hour is reported, but at 650 °C in undiluted feed [27]. Such a value would be reached at 570 °C using our catalysts with an activation energy of 60 kJ/mol.

The long-term stability of catalytic activity was not yet studied. Some tests, done with ceria–zirconia catalyst, have shown no significant decrease in propane conversion for a 4-h time on stream at 450 °C.

4. Summary

A 1 wt% rhodium on alumina, titania, and ceria–zirconia catalysts was coated on stainless-steel sheets by dip-coating in very stable colloidal dispersions of nanoparticles in water. According to the support, the porosity and the specific surface area of films formed after a calcination at 500 °C, ranged from 50% and 300 m^2/g for alumina xerogels to 25% and 60 m^2/g for titania. This low porosity can be strongly enhanced by addition of PEG 2000 in the titania and ceria–zirconia sols. Besides the PEG addition eliminated the film cracking observed without additive with titania and ceria–zirconia layers.

The best catalytic activity for steam reforming of propane was observed for titania and ceria–zirconia supports for which the propane conversion started at 250 °C against 320 °C for alumina carrier. At 350 °C propane conversion was more than three times better than the conversion measured on alumina catalyst. When the thickness of the ceria–zirconia and titania films was increased, the conversion did not increase accordingly, probably because the porosity was too low for the lower part of the layers to work efficiently. Indeed, addition of PEG, which strongly increases the porosity, eliminated this impediment. However, in the case of titania support, addition of PEG did not improve the reaction rate despite the large increase of surface area.

At 500 °C, whatever the catalyst support, a first-order kinetics was found with respect to propane. Though much work remains to be done, this preliminary study shows that it could be possible with these thin layers of sol–gel catalysts coated on corrugated-steel sheets to build cheap but efficient fuel processors suitable for large-scale production.

Acknowledgments

This research was supported by the French Environment and Energy Management Agency ADEME (http://www2.ademe.fr) through the PREPAC project (collaboration EIfER, LIEBHERR Aerospace, LGC, CIRIMAT, IRCELYON, ICB). The Fermat Federation (http://www.federation-fermat.org) is also gratefully acknowledged for funding the mass spectrometer acquisition.

References

[1] M. Krumpelt, T.R. Krause, J.D. Carter, J.P. Kopasz, S. Ahmed, Catal. Today 77 (2002) 3–16.
[2] K. Ahmed, J. Gamman, K. Foger, Solid State Ionics 152–153 (2002) 485–492.
[3] F. Joensen, J.R. Rostrup-Nielsen, J. Power Sources 105 (2002) 195–201.
[4] A. Heinzel, J. Roes, H. Brandt, J. Power Sources 145 (2005) 312–318.
[5] K. Eguchi, H. Kojo, T. Takeguchi, R. Kikuchi, K. Sasaki, Solid State Ionics 152–153 (2002) 411–416.
[6] K. Haas-Santo, M. Fichtner, K. Schubert, Appl. Catal. A 220 (2001) 79–92.
[7] G. Kolb, V. Hessel, Chem. Eng. J. 98 (2004) 1–38.
[8] J. Thormann, P. Pfeifer, K. Schubert, U. Kunz, Chem. Eng. J. 135S (2008) S74–S81.
[9] P. Reuse, A. Renken, K. Haas-Santo, O. Gorke, K. Schubert, Chem. Eng. J. 101 (2004) 133–141.
[10] J.R. Rostrup-Nielsen, J.H. Bak Hansen, J. Catal. 144 (1993) 38–49.
[11] J. Wei, E. Iglesia, J. Phys. Chem. B 108 (2004) 4094–4103.
[12] B.E. Yoldas, J. Mater. Sci. 10 (1975) 1856–1860.
[13] B.E. Yoldas, Am. Ceram. Soc. Bull. 54 (1975) 286–288.
[14] B.E. Yoldas, Am. Ceram. Soc. Bull. 54 (1975) 289–290.
[15] A.S. Deshpande, N. Pinna, P. Beato, M. Antonietti, M. Niederberger, Chem. Mater. 16 (2004) 2599–2604.
[16] F. Bosc, A. Ayral, P.A. Albouy, C. Guizard, Chem. Mater. 15 (2003) 2463–2468.
[17] G. Oskam, A. Nellore, R.L. Penn, P.C. Searson, J. Phys. Chem. B 107 (2003) 1734–1738.
[18] J. Rodríguez-Carvajal, Commission Powder Diffraction (IUCr) Newsl. 26 (2001) 12–19.
[19] A.L. Patterson, Phys. Rev. 56 (1939) 978–982.
[20] S. Brunauer, P. Hemmett, E. Teller, J. Am. Chem. Soc. 60 (1938) 309–319.
[21] N. Seaton, J. Walton, N. Quirke, Carbon 27 (1989) 853–861.
[22] J.R. Rostrup-Nielsen, Steam Reforming Catalysts, Danish Technical Press Inc, 1975.
[23] P. Alphonse, M. Courty, Thermochim. Acta 425 (2005) 75–89.
[24] H. Zhang, J.F. Banfield, J. Phys. Chem. B 104 (2000) 3481–3487.
[25] T. Miki, K. Nishizawa, K. Suzuki, K. Kato, J. Mater. Sci. 39 (2004) 699–701.
[26] F. Bosc, A. Ayral, N. Keller, V. Keller, Appl. Catal. B 69 (2007) 133–137.
[27] G. Kolb, R. Zapf, V. Hessel, H. Lowe, Appl. Catal. A 277 (2004) 155–166.
[28] P.O. Graf, B.L. Mojet, J.G. van Ommen, L. Lefferts, Appl. Catal. A 332 (2007) 310–317.
[29] P. van Beurden, On the Catalytic Aspects of Steam-Methane Reforming, Energy Research Centre of the Netherlands (ECN), Technical Report I-04-003, 2004. Available from: <http://www.ecn.nl/docs/library/report/2004/i04003.pdf>.
[30] J. Wei, E. Iglesia, J. Catal. 224 (2004) 370–383.
[31] J. Wei, E. Iglesia, J. Catal. 225 (2004) 116–127.